Supporting Information

Unraveling Interfacial Electron Transfer Dynamics in Noble Metal Cocatalyst Modified Ferroelectric Photocatalysts via Nonadiabatic Molecular Dynamics Simulations

Jian-An Liu, [ab] Li-Chang Yin,[*ab] Lianzhou Wang, [c] and Gang Liu[*ab]

[a] Shenyang National Laboratory for Materials Science, Institute of Metal Research, Chinese Academy of Sciences, 72 Wenhua Road, Shenyang 110016, China.

[b] School of Materials Science and Engineering, University of Science and Technology of China, 72 Wenhua Road, Shenyang 110016, China.

[c] Nanomaterials Centre, School of Chemical Engineering and Australian Institute for Bioengineering and Nanotechnology, The University of Queensland, QLD 4072, Australia.

*Correspondence: lcyin@imr.ac.cn (LCY); gangliu@imr.ac.cn (GL)

1. Computational Details

Our NAMD simulations use the density functional theory (DFT) as implemented in the Vienna ab initio simulation package (VASP) to carry out the static and ab initio molecular dynamics calculations.[1] The electron-nuclear interactions were described by using the projector-augmented wave potentials,[2] and the exchange-correlation interaction was described by generalized gradient approximation (GGA) with the Perdew-Burke-Ernzerhof functional.[3] To overcome the well-known self-interaction error in DFT, the GGA + U method was used to treat the *d* electrons of Ti and Nb atoms and the *2p* electrons of O atoms (U = 5.0 eV for Ti-*3d*, U = 5.0 eV for Nb-*4d*, and U = 8 eV for O-*2p*).[4] To construct the Bi_3TiNbO_9/noble metal (BTNO/NM) composite interfaces (BTNO/Rh, BTNO/Pd, and BTNO/Pt), the NM(100) surfaces with a thickness of three atomic layers were attached to the BTNO(001) surface that contains a bottom $(Bi_2O_2)^{2+}$ atomic layer and an upper perovskite $(BiTiNbO_7)^{2-}$ atomic layer. The bottom Bi atoms were passivated with Cl atoms. It should be noted that this BTNO(001) slab can effectively capture the essential structural and electronic characteristics of BTNO, thereby working as a reasonable structure model for constructing the BTNO/NM interfaces. Accordingly, the resulting BTNO/NM interfaces provide a reliable platform for accurately investigating interfacial properties relevant to the interfacial electron transfer (IET) dynamics.

For all slabs, a vacuum with a thickness of 15 Å was set along the *z* direction. Notably, a 2×2 supercell of these BTNO/NM interfaces with a 2×2×1 k-point mesh was adopted for all DFT calculations and NAMD simulations. For all NM cocatalysts, a

conventional unit cell and an 8×8×8 k-point mesh were adopted. The plane wave energy cutoff was set to be 400 eV. All geometries were fully relaxed with the convergence criterion of 10^{-5} eV and 0.02 eV·Å^{-1} for the total energy and residual force, respectively.

The ab initio NAMD simulations were performed by using the Hefei-NAMD code.[5] After geometry optimization, the temperature of these BTNO/NM interfaces was brought to 300 K by using velocity rescaling.[6] Subsequently, a microcanonical ab initio molecular dynamics trajectory of 4 ps is then generated with a time step of 1 fs. The NAMD results were obtained by averaging over 100 different initial configurations selected from the molecular dynamics trajectory based on the classical path approximation.[7] For each chosen structure, 2×10^4 trajectories were sampled for the last 2 ps.

The lattice mismatch (δ) for the BTNO/NM interfaces was calculated by using the following equation,

$$\delta = \frac{|a_2 - a_1|}{a_1}$$

where a_1 and a_2 are the lattice constants of the BTNO(001) surface and the specific surface of NM cocatalysts, respectively. To evaluate the structural stability for these BTNO/NM interfaces, the interfacial binding energy (ΔE) was calculated based on the following equation,

$$\Delta E = \frac{1}{S}(E_{\mathrm{BTNO/NM}} - E_{\mathrm{BTNO}} - E_{\mathrm{NM}})$$

where S is the surface area of the BTNO/NM interfaces. $E_{\mathrm{BTNO/NM}}$, E_{BTNO}, and E_{NM} are the DFT energies of the BTNO/NM interfaces, the BTNO(001) surface, and the NM(100) surfaces, respectively.

2. Supplementary Figures and Tables

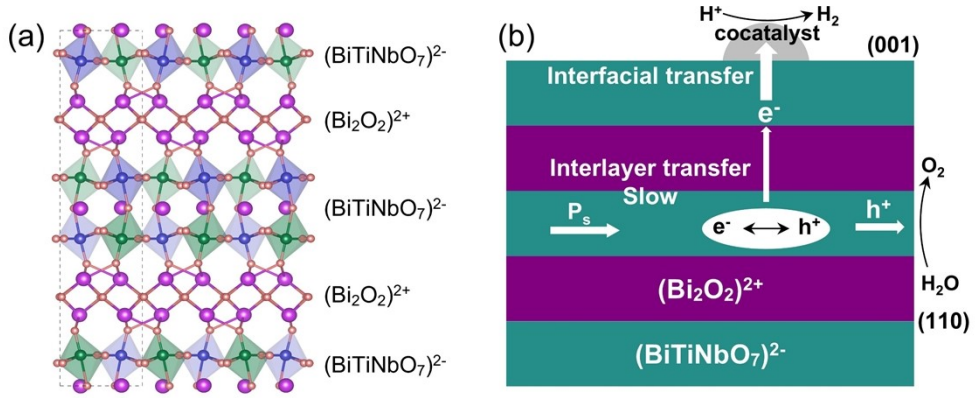

Fig. S1 (a) Atomic structure of the typical layered Aurivillius compounds, BTNO. The purple, green, blue, and red balls denote the Bi, Ti, Nb, and O atoms, respectively. (b) Schematic of the photogenerated charge transfer and migration process in BTNO.

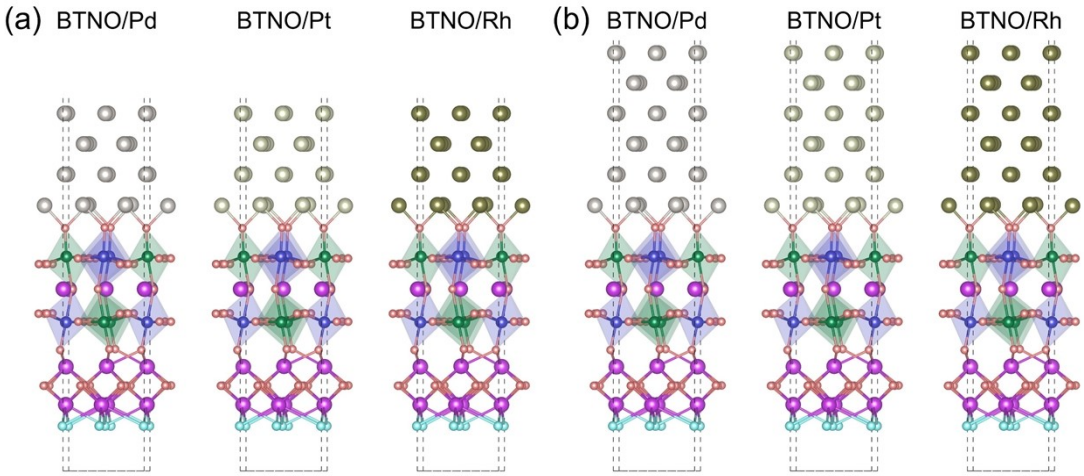

Fig. S2 Atomic structures for BTNO/NM interfaces with (a) four and (b) six NM atomic layers. The purple, green, blue, red, cyan, grey, yellow, and brown balls denote the Bi, Ti, Nb, O, Cl, Pd, Pt, and Rh atoms, respectively.

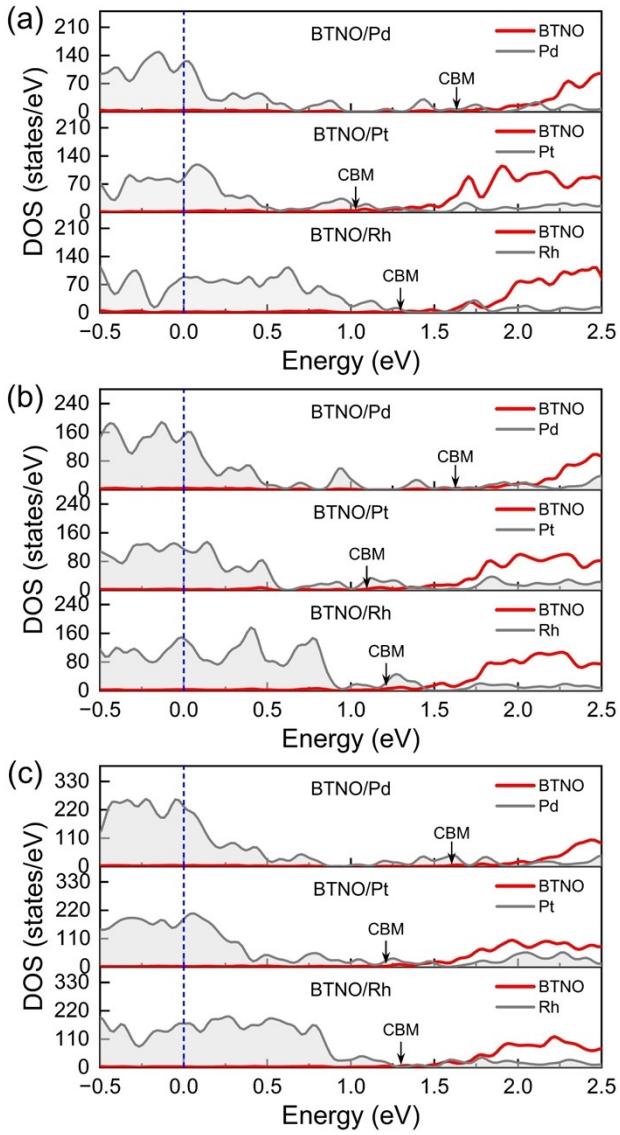

Fig. S3 Projected density of states (DOS) for the BTNO/NM composites with (a) three, (b) four, and (c) six NM atomic layers. The Fermi level (E_F) of composite photocatalysts is denoted by blue dashed line and set to be 0 eV.

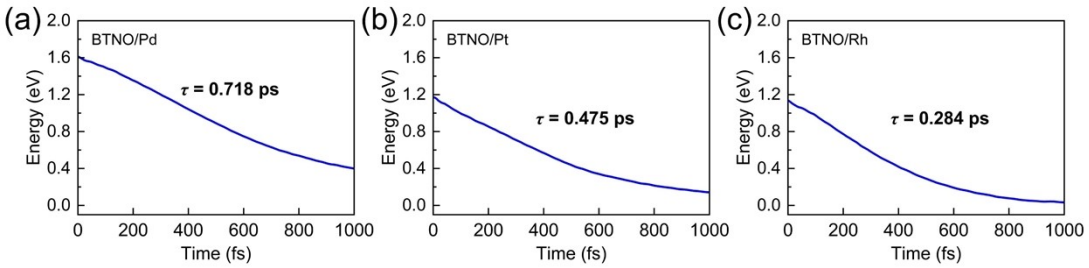

Fig. S4 Time-dependent averaged electron energies for (a) BTNO/Pd, (b) BTNO/Pt, and (c) BTNO/Rh interfaces with four NM atomic layers. The energy reference is the averaged Fermi energy. The fitted IET time (τ) is also given for each composite.

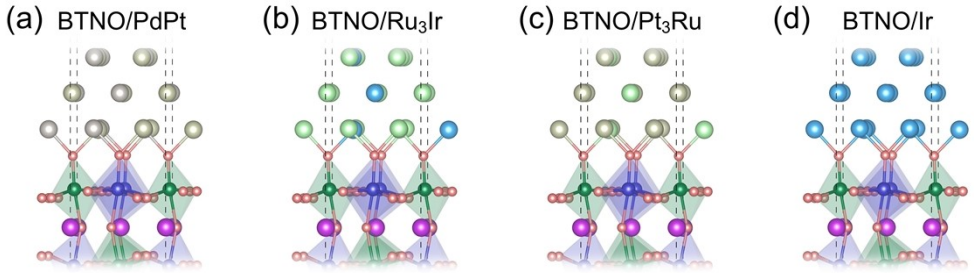

Fig. S5 Atomic structures of (a) BTNO/PdPt, (b) BTNO/Ru_3Ir, (c) BTNO/ Pt_3Ru, and (d) BTNO/Ir interfaces. The purple, green, blue, red, grey, yellow, light green, and light blue balls denote the Bi, Ti, Nb, O, Pd, Pt, Ru, and Ir atoms, respectively.

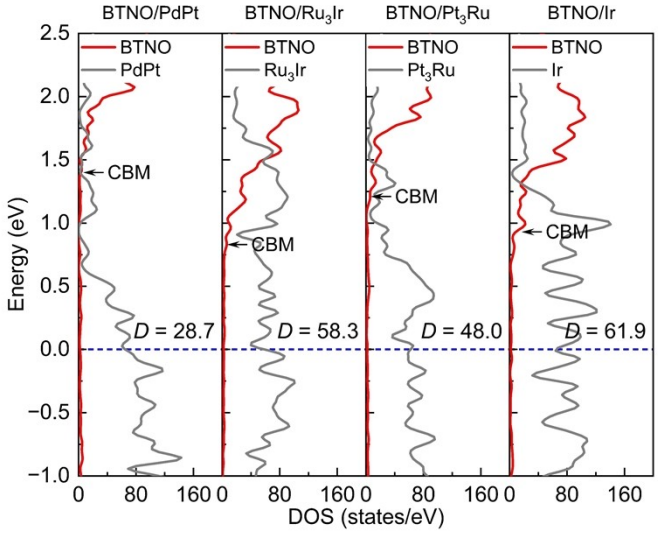

Fig. S6 Projected DOS for BTNO/PdPt, BTNO/Ru_3Ir, BTNO/Pt_3Ru, and BTNO/Ir

composites. The E_F of each composite is denoted by blue dashed line and set to be 0 eV. The averaged DOS (D) energy region between the CBM of BTNO and the E_F of composite is also given for each composite.

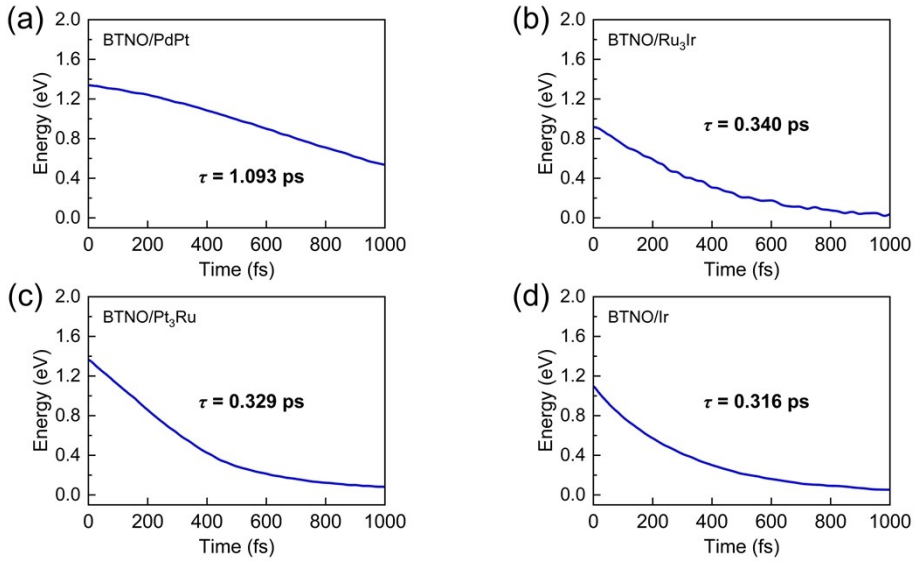

Fig. S7 Time-dependent averaged electron energies for (a) BTNO/PdPt, (b) BTNO/Ru_3Ir, (c) BTNO/Pt_3Ru, and (d)BTNO/Ir composites. The energy reference is the averaged Fermi energy. The IET time (τ) is also given for each composite.

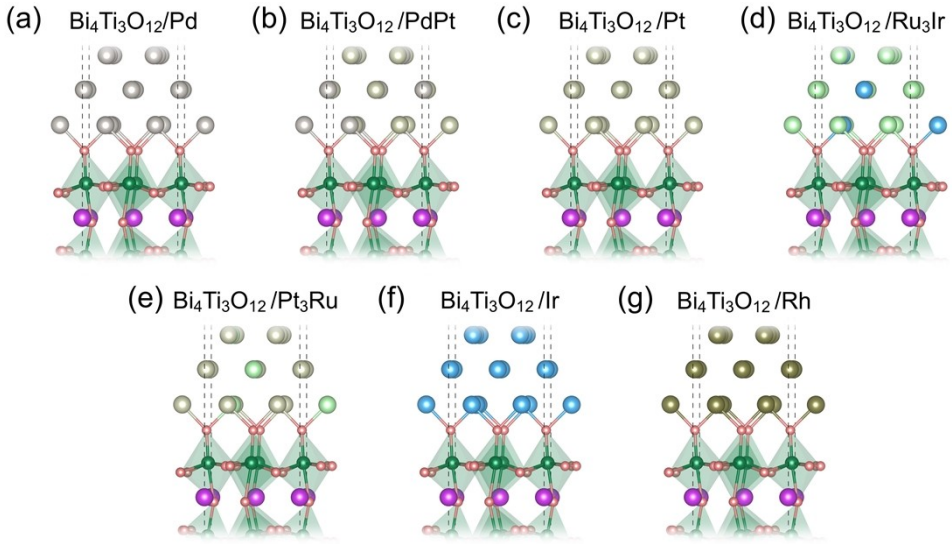

Fig. S8 Atomic structures of (a) $Bi_4Ti_3O_{12}$/Pd, (b) $Bi_4Ti_3O_{12}$/PdPt, (c) $Bi_4Ti_3O_{12}$/Pt, (d)

$Bi_4Ti_3O_{12}/Ru_3Ir$, (e) $Bi_4Ti_3O_{12}/Pt_3Ru$, (f) $Bi_4Ti_3O_{12}/Ir$, and (g) $Bi_4Ti_3O_{12}/Rh$ composites. The purple, green, red, grey, yellow, light green, light blue, and brown balls denote the Bi, Ti, O, Pd, Pt, Ru, Ir, and Rh atoms, respectively

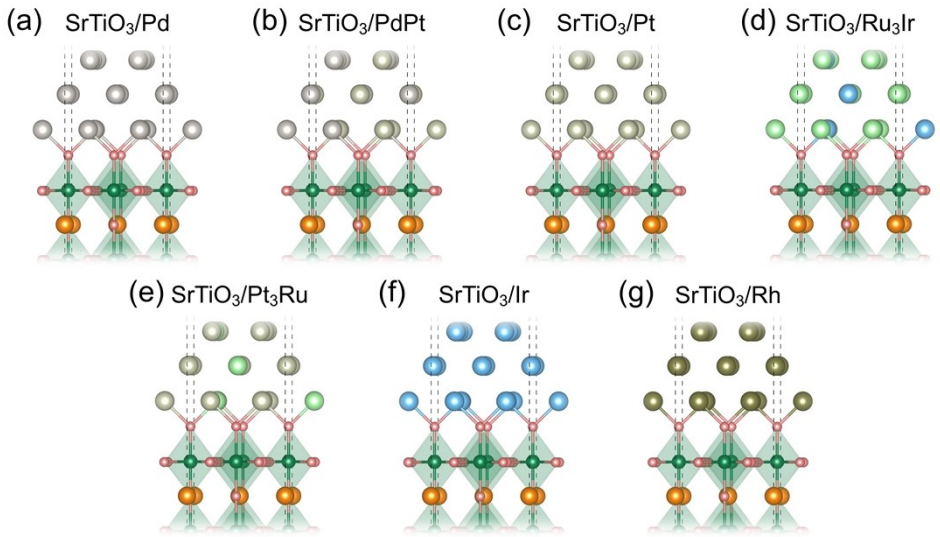

Fig. S9 Atomic structures of (a) $SrTiO_3$/Pd, (b) $SrTiO_3$/PdPt, (c) $SrTiO_3$/Pt, (d) $SrTiO_3/Ru_3Ir$, (e) $SrTiO_3$/ Pt_3Ru, (f) $SrTiO_3$/Ir, and (g) $SrTiO_3$/Rh composites. The orange, green, red, grey, yellow, light green, light blue, and brown balls denote the Sr, Ti, O, Pd, Pt, Ru, Ir, and Rh atoms, respectively.

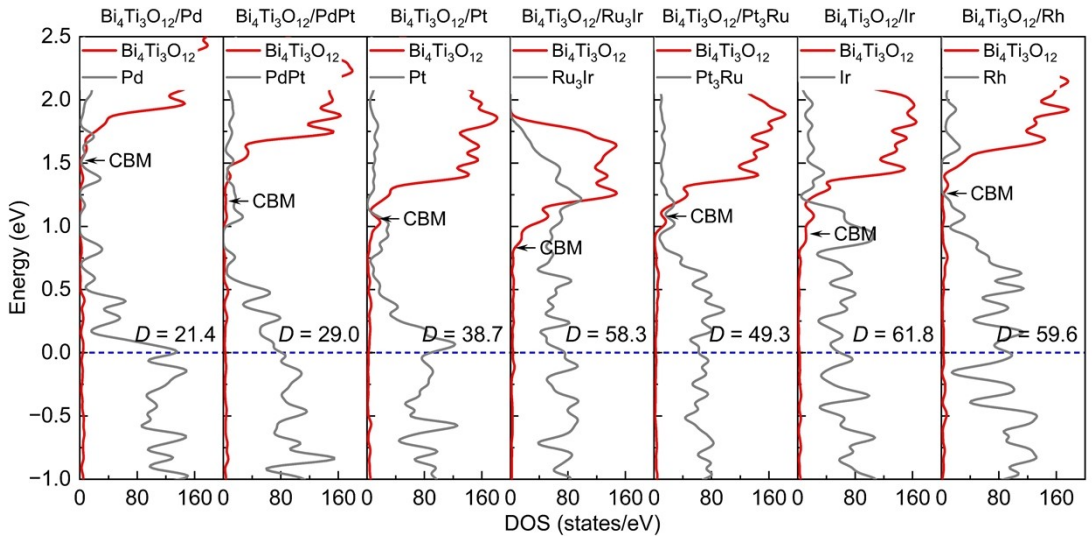

Fig. S10 Projected DOS for $Bi_4Ti_3O_{12}$/NM composite: $Bi_4Ti_3O_{12}$/Pd, $Bi_4Ti_3O_{12}$/PdPt,

$Bi_4Ti_3O_{12}$/Pt, $Bi_4Ti_3O_{12}$/Ru_3Ir, $Bi_4Ti_3O_{12}$/Pt_3Ru, $Bi_4Ti_3O_{12}$/Ir, and $Bi_4Ti_3O_{12}$/Rh. The E_F of each composite is denoted by blue dashed line and set to be 0 eV. The D value is also given for each composite.

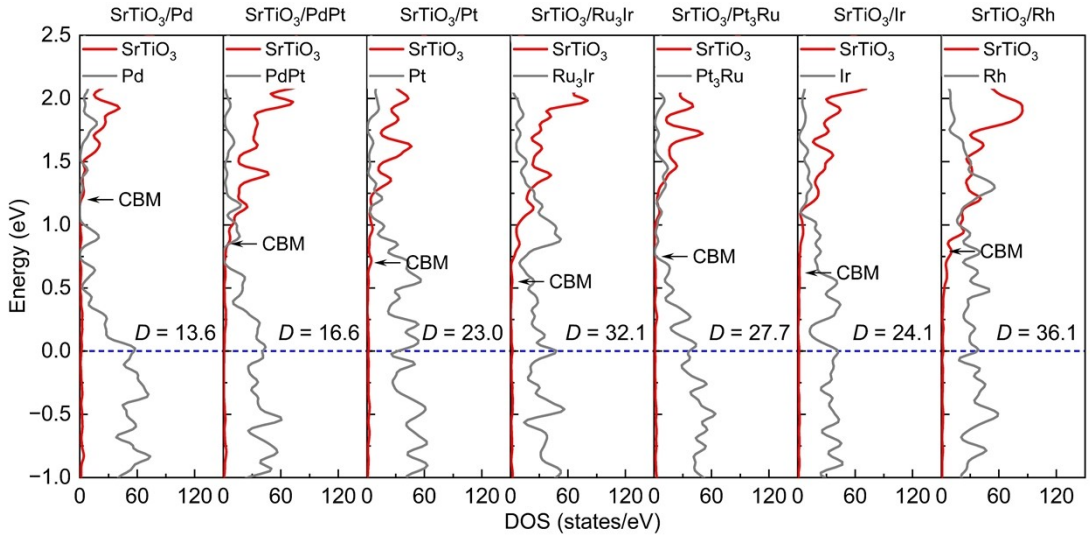

Fig. S11 Projected DOS for $SrTiO_3$/NM composite: $SrTiO_3$/Pd, $SrTiO_3$/PdPt, $SrTiO_3$/Pt, $SrTiO_3$/Ru_3Ir, $SrTiO_3$/ Pt_3Ru, $SrTiO_3$/Ir, and $SrTiO_3$/Rh. The E_F of each composite is denoted by blue dashed line and set to be 0 eV. The D value is also given for each composite.

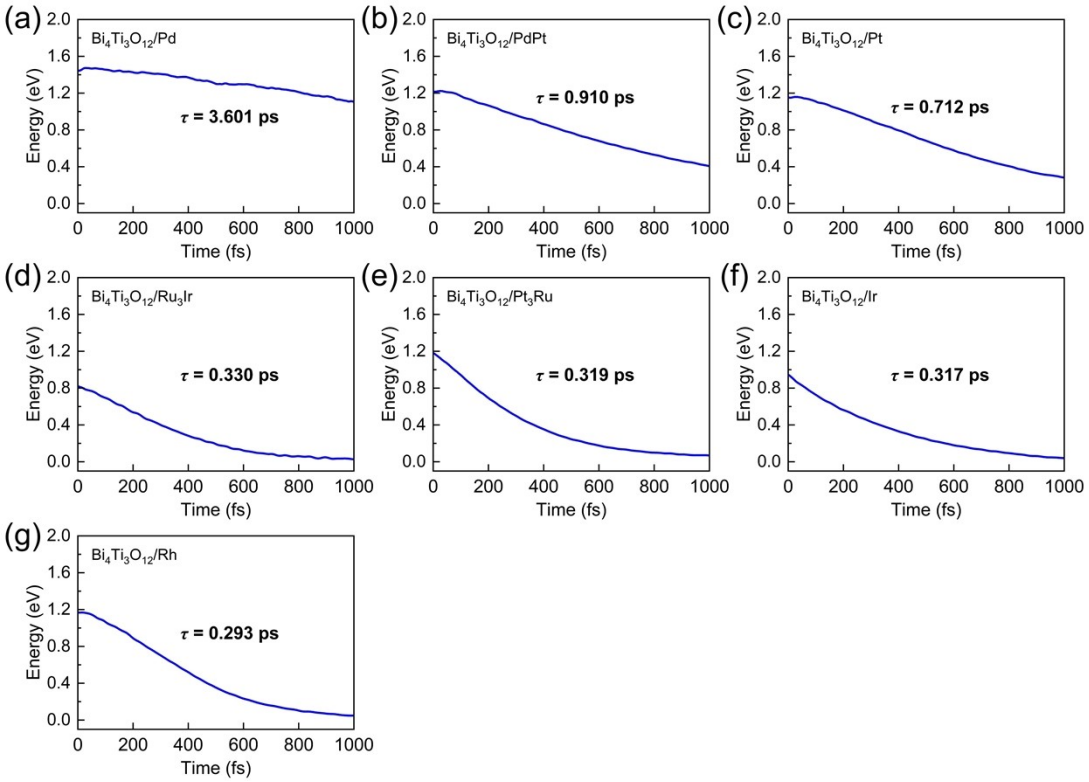

Fig. S12 Time-dependent averaged electron energies for (a) $Bi_4Ti_3O_{12}$/Pd, (b) $Bi_4Ti_3O_{12}$/PdPt, (c) $Bi_4Ti_3O_{12}$/Pt, (d) $Bi_4Ti_3O_{12}$/Ru_3Ir, (e) $Bi_4Ti_3O_{12}$/Pt_3Ru, (f) $Bi_4Ti_3O_{12}$/Ir, and (g) $Bi_4Ti_3O_{12}$/Rh composites. The energy reference is the averaged Fermi energy. The IET time (τ) is also given for each composite.

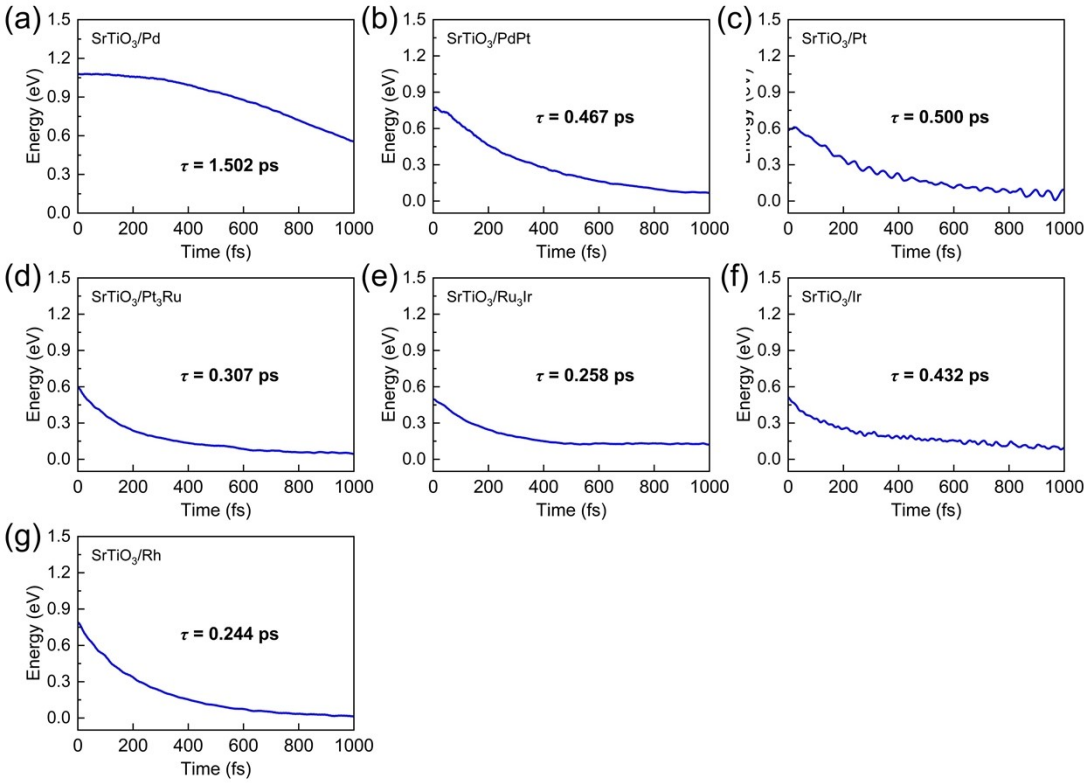

Fig. S13 Time-dependent average electron energies for (a) $SrTiO_3$/Pd, (b) $SrTiO_3$/PdPt, (c) $SrTiO_3$/Pt, (d) $SrTiO_3$/Ru_3Ir, (e) $SrTiO_3$/ Pt_3Ru, (f) $SrTiO_3$/Ir, and (g) $SrTiO_3$/Rh composites. The energy reference is the averaged Fermi energy. The IET time (τ) is also given each composite.

Table S1 The calculated lattice constants for the (100), (110), and (111) surfaces of NM cocatalysts (Pd, Pt, and Rh).

	Pd	Pt	Rh
(100)	a = 5.57 Å b = 5.57 Å	a = 5.61 Å b = 5.61 Å	a = 5.41 Å b = 5.41 Å
(110)	a = 5.57 Å b = 3.94 Å	a = 5.61 Å b = 3.97 Å	a = 5.41 Å b = 3.82 Å
(111)	a = 4.83 Å b = 2.79 Å	a = 4.86 Å b = 2.81 Å	a = 4.68 Å a = 2.70 Å

Table S2 The lattice mismatches along the *a* and *b* directions for the BTNO/NM interfaces composed of the BTNO(001) surface and the low-index (100), (110), or (111) surfaces of NM cocatalysts. The lattice constants of the BTNO(001) surface were calculated to be a = 5.53 Å and b = 5.46 Å.

	BTNO/Pd	BTNO/Pt	BTNO/Rh
BTNO(001)/NM(100)	0.7%, 2.0%	1.4%, 2.7%	2.2%, 0.9%
BTNO(001)/NM(110)	6.4%, 2.0%	6.9%, 2.7%	3.5%, 0.9%
BTNO(001)/NM(111)	13%, 0.7%	12%, 1.4%	17%, 2.2%

Note: The BTNO(001)/NM(100), BTNO(001)/NM(110), and BTNO(001)/NM(111) interfaces are constructed by using a conventional unit cell of BTNO(001) surface and a conventional unit cell of NM(100) surfaces, a 2×1 supercell of BTNO(001) surface and a 1×3 supercell of NM(110) surfaces, and a conventional unit cell of BTNO(001) surface and a 1×2 supercell of the NM(111) surfaces, respectively.

Table S3 The calculated interfacial binding energies (meV/Å^2) of BTNO(001)/NM(100) interfaces with various NM slab thicknesses.

	BTNO/Pd	BTNO/Pt	BTNO/Rh
Three NM atomic layers	-167	-168	-184
Four NM atomic layers	-164	-164	-178
Six NM atomic layers	-163	-163	-178

Table S4 The lattice constants of relevant surfaces used for constructing the corresponding BTNO/NM, $Bi_4Ti_3O_{12}$/NM, and $SrTiO_3$/NM composites.

	BTNO(001)	$Bi_4Ti_3O_{12}$(001)	$SrTiO_3$(001)	
Semiconductor	a = 5.53 Å b = 5.46 Å	a = 5.57 Å b = 5.52 Å	a = b = 5.59 Å	
NM	Pd(100)	Pt(100)	Rh(100)	Ir(100)
	a = b = 5.57 Å	a = b = 5.61 Å	a = b = 5.41 Å	a = b = 5.48 Å
	PdPt(100)	Pt_3Ru(100)	Ru_3Ir(100)	FeCo(100)
	a = b = 5.60 Å	a = b = 5.57 Å	a = b = 5.41 Å	a = b = 5.06 Å

Table S5 The lattice mismatches along the *a* and *b* directions for the BTNO/NM, $Bi_4Ti_3O_{12}$/NM, and $SrTiO_3$/NM interfaces, which were constructed by using relevant surfaces detailed in Table S4.

	BTNO(001)	$Bi_4Ti_3O_{12}$(001)	$SrTiO_3$(001)
Pd(100)	0.7%, 2.0%	0.1%, 1.0%	0.2%, 0.2%
Pt(100)	1.4%, 2.7%	0.8%, 1.7%	0.5%, 0.5%
Rh(100)	2.2%, 0.9%	2.9%, 2.0%	3.2%, 3.2%
Ir(100)	0.8%, 0.3%	1.6%, 0.7%	1.9%, 1.9%
PdPt(100)	1.3%, 2.7%	0.6%, 1.6%	0.3%, 0.3%
Pt_3Ru(100)	1.6%, 1.9%	0.1%, 0.9%	0.4%, 0.4%
Ru_3Ir(100)	2.3%, 1.0%	2.9%, 2.0%	3.2%, 3.2%
FeCo(100)	8.6%, 7.3%	9.2%, 8.3%	9.4%, 9.4%

References

(1) Kresse, G.; Furthmüller, J. Efficient Iterative Schemes for Ab Initio Total-Energy Calculations Using a Plane-Wave Basis Set. *Physical Review B* **1996**, *54* (16), 11169-11186.

(2) Kresse, G.; Joubert, D. From Ultrasoft Pseudopotentials to the Projector Augmented-Wave Method. *Physical Review B* **1999**, *59* (3), 1758-1775.

(3) Perdew, J. P.; Burke, K.; Ernzerhof, M. Generalized Gradient Approximation Made Simple. *Phys. Rev. Lett.* **1996**, *77* (18), 3865-3868.

(4) Anisimov, V. I.; Zaanen, J.; Andersen, O. K. Band theory and Mott insulators: Hubbard U instead of Stoner I. *Physical Review B* **1991**, *44* (3), 943-954.

(5) Zheng, Q.; Chu, W.; Zhao, C.; Zhang, L.; Guo, H.; Wang, Y.; Jiang, X.; Zhao, J.

Ab Initio Nonadiabatic Molecular Dynamics Investigations on the excited Carriers in Condensed Matter Systems. *WIREs Comput. Mol. Sci.* **2019**, *9* (6), e1411.

(6) Bussi, G.; Donadio, D.; Parrinello, M. Canonical Sampling through Velocity Rescaling. *The Journal of Chemical Physics* **2007**, *126* (1), 014101.

(7) Tully, J. C. Mixed Quantum-Classical Dynamics: Mean-Field and Surface-Hopping. In *Classical and Quantum Dynamics in Condensed Phase Simulations*, WORLD SCIENTIFIC, 1998; pp 489-514.